PHYSICAL REVIEW B **87**, 140503(R) (2013)

High-temperature surface superconductivity in rhombohedral graphite

N. B. Kopnin,[1,2] M. Ijäs,[3] A. Harju,[3] and T. T. Heikkilä[1]
[1]*Low Temperature Laboratory, Aalto University, P.O. Box 15100, FI-00076 Aalto, Finland*
[2]*L. D. Landau Institute for Theoretical Physics, 117940 Moscow, Russia*
[3]*COMP Centre of Excellence and Helsinki Institute of Physics, Department of Applied Physics, Aalto University, P.O. Box 14100, FI-00076 Aalto, Finland*

(Received 26 October 2012; published 9 April 2013)

Surface superconductivity in rhombohedral graphite is a robust phenomenon which can exist even when higher order hoppings between the layers lift the topological protection of the surface flat band and introduce a quadratic dispersion of electrons with a heavy effective mass. We show that for weak pairing interaction, the flat-band character of the surface superconductivity transforms into a BCS-like relation with high critical temperature characterized by a higher coupling constant due to a much larger density of states than in the bulk. Our results offer an explanation for the recent findings of graphite superconductivity with an unusually high transition temperature.

DOI: 10.1103/PhysRevB.87.140503 PACS number(s): 74.20.Pq, 74.70.Wz

The relation between the critical temperature and the coupling strength depends on the density of states (DOS) near the Fermi surface; it becomes stronger as the energy dispersion gets weaker, boosting the superconductivity. The extreme case would be a completely dispersionless energy spectrum, a flat band, which has been predicted in many condensed matter systems; see, e.g., Refs. 1–4. In some cases the flat bands are protected by topology in momentum space; they emerge in gapless topological matter.[5–13] A singular DOS associated with the dispersionless spectrum was recently shown[14] to essentially enhance the transition temperature opening a new route to room-temperature superconductivity. The problem is to find the metal with such a higher order dispersion around the Fermi sea. References 9,14, and 15 show that within the nearest-neighbor approximation, rhombohedral graphite (RHG) has topologically protected surface states with a flat band at the Fermi energy, and these surface states support high-temperature superconductivity with T_c linear in the pairing strength, where the superconducting order parameter is concentrated around the surfaces. A flat band forms out of a low dispersive band that appears on the surface of a multilayered rhombohedral graphene structure with a large number of layers.

Experimental evidence of a high-temperature superconductivity in graphite in the form of a small Meissner effect and of a sharp drop in resistance appeared during the past years.[16,17] Recently, these findings have been ratified by observations of zero resistance in graphitic samples up to 175 K[18] and indications of even room-temperature superconductivity in specially prepared graphite samples.[19] In Ref. 14 the high-temperature superconductivity in graphite was related to surface superconductivity that may form either on the outer surfaces of the sample or on twin boundaries of or on grain boundaries between inclusions of RHG. In the present Rapid Communication we confirm this scenario and demonstrate that the surface superconductivity is a robust phenomenon which survives even when the topological protection of the flat band is lifted. In particular, the next-nearest-neighbor hoppings in RHG break the topological protection and, therefore, the flat-band mechanism of superconductivity could be destroyed. However, we show (see also Ref. 20) that, though breaking the flat-band scenario for sufficiently low pairing potentials, these higher order interactions provide another mechanism of surface superconductivity which is of the BCS type but still has a much larger coupling constant than the usual superconductivity in bulk. The enhanced coupling constant comes from a high DOS of heavy surface quasiparticles emerging on the background of the preexisting flat band.

Electron dispersion. The RHG lattice and the tight-binding couplings are depicted in Fig. 1 (left panel). The layers are labeled by n (from the bottom), the atoms A in layer n are on top of atoms B in layer $n-1$, and d is the interlayer distance. The tight-binding parameters satisfy[21] $\gamma_0 \gg \gamma_1 \sim \gamma_3 \gg \gamma_4$. In the numerics below, we use $\gamma_0 = 2.58$ eV, $\gamma_1 = 0.34$ eV, $\gamma_3 = 0.17$ eV, and $\gamma_4 = 0.04$ eV, which give the best fit to the density functional theory (DFT) calculation of the surface state dispersion.[22]

The RHG is a multilayered graphene structure. The conical spectrum near the Dirac points $\mathbf{K}$ and $\mathbf{K}'$ of the Brillouin zone of a single-layer graphene (for details, see Ref. 21, and references therein) is transformed into low-dispersion, low-energy bands (see Fig. 1, right) which determine the unique features of this system. Being interested in low energies, we concentrate on in-plane momenta $\mathbf{p} = (p_x, p_y)$ close to one of these Dirac corners. A standard Fourier series expansion near $\mathbf{K}$ yields[20]

$$H_{\mathbf{K}} = \sum_{\mathbf{p}} \sum_{m,n=1}^{N} \hat{\psi}_m^{\dagger}(\mathbf{p}) \hat{H}_{mn}(\mathbf{K},\mathbf{p}) \hat{\psi}_n(\mathbf{p}), \tag{1}$$

where $\hat{H}_{mn}(\mathbf{K},\mathbf{p}) = \sum_{l=0}^{4} \hat{H}_{mn}^{(l)}(\mathbf{K},\mathbf{p})$ and

$$\hat{H}_{mn}^{(0)}(\mathbf{K},\mathbf{p}) = v_F(\hat{\boldsymbol{\sigma}} \cdot \mathbf{p})\delta_{mn},$$
$$\hat{H}_{mn}^{(1)}(\mathbf{K},\mathbf{p}) = -\gamma_1 \left[e^{-i\frac{\pi}{6}} \hat{\sigma}_+ \delta_{m,n+1} + e^{i\frac{\pi}{6}} \hat{\sigma}_- \delta_{m,n-1} \right],$$
$$\hat{H}_{mn}^{(3)}(\mathbf{K},\mathbf{p}) = \tilde{\gamma}_3 v_F \left[e^{-i\frac{\pi}{3}} \hat{\sigma}_+ p_+ \delta_{m,n-1} + e^{i\frac{\pi}{3}} \hat{\sigma}_- p_- \delta_{m,n+1} \right],$$
$$\hat{H}_{mn}^{(4)}(\mathbf{K},\mathbf{p}) = \tilde{\gamma}_4 v_F \left[e^{i\frac{\pi}{6}} p_- \delta_{m,n-1} + e^{-i\frac{\pi}{6}} p_+ \delta_{m,n+1} \right].$$

Here $\tilde{\gamma}_3 = \gamma_3/\gamma_0$, $\tilde{\gamma}_4 = \gamma_4/\gamma_0$, $p_\pm = p_x \pm i p_y = p e^{\pm i\phi}$, and $v_F = 3a_0\gamma_0/2\hbar$. The Pauli matrices $\hat{\boldsymbol{\sigma}}$ and $2\hat{\sigma}_\pm = \hat{\sigma}_x \pm i\hat{\sigma}_y$ act on pseudospinors $\hat{\psi}_n = (\psi_n^1, \psi_n^2)^T$, $\hat{\psi}_n^{\dagger} = (\psi_n^{1*}, \psi_n^{2*})$, where $\psi_n^1 = \psi_n^A$, $\psi_n^2 = e^{i\pi/6}\psi_n^B$.

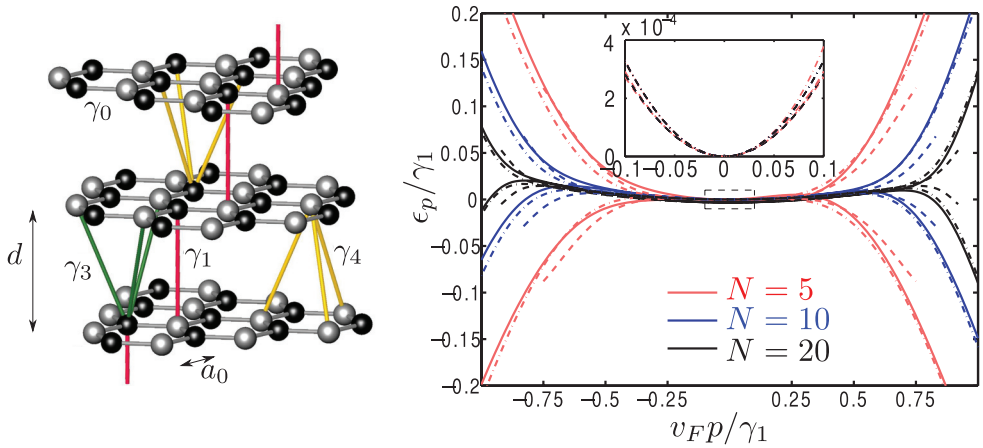

FIG. 1. (Color online) Left: Rhombohedral graphite. The black and gray atoms correspond to A and B sites, respectively. Right: Cuts of the 3d spectrum for $p < p_{\rm FB} \equiv \gamma_1/v_F$ along the K-Γ (K-M) on negative (positive) x axis; $N = 5$ (red), $N = 10$ (blue), and $N = 20$ (black) graphene layers. The DFT calculations are shown in full, tight-binding in dash-dotted, and Eq. (6) in dashed lines (the latter plotted up to their regimes of applicability). The inset is a zoom-up of the low-energy region with tight-binding (dash-dotted) and analytical (dashed) curves. The deviations between the dashed and other lines show up when ξ_p becomes dominant in Eq. (6), and are partially due to γ_3 neglected there.

To construct the associated Bogoliubov–de Gennes (BdG) Hamiltonian for the superconducting state we need also the time-reversed "hole" Hamiltonian at $\mathbf{K}$. It follows from the particle Hamiltonian in a vicinity of the opposite Dirac point $-\mathbf{K}$ which is equivalent to $\mathbf{K}'$. The wave function $\psi^h_{\mathbf{K}}$ of a hole excitation near $\mathbf{K}$ is $\psi^h_{\mathbf{K}} = \bar{\psi}^*_{-\mathbf{K}}$. One can check that the hole Hamiltonian is $H^h_{mn}(\mathbf{K},\mathbf{p}) = H^*_{mn}(-\mathbf{K},-\mathbf{p})$. Therefore, $H^h_{\mathbf{K}}$ has the form of Eq. (1) where $\hat{\psi}_n(\mathbf{p})$ are replaced with $\hat{\psi}^{(h)}_n(\mathbf{p})$. In what follows, we denote the electron wave function by $\hat{u}_n = \hat{\psi}_n$ and the hole wave function by $\hat{v}_n = \hat{\psi}^h_n$.

Low-energy spectrum in the normal state. Here we study the normal state using Hamiltonian Eq. (1) and the relative magnitudes of the coupling constants listed above. The Schrödinger equation takes the form

$$\sum_m \hat{H}_{nm}(\mathbf{K},\mathbf{p})\hat{u}_m(\mathbf{p}) = (\epsilon+\mu)\hat{u}_n(\mathbf{p}). \tag{2}$$

The energy is measured from the chemical potential μ. The energy spectrum in bulk is obtained by ignoring the outermost layers $n = 1$ and N and using the ansatz $\hat{u}_n \propto e^{ip_z dn}$, where p_z is out-of-plane momentum. For zero doping $\mu = 0$ and for $\gamma_3 = \gamma_4 = 0$, the Fermi surface, $\epsilon(p,p_z,\phi) = 0$, shrinks to a spiral line $v_F p = \gamma_1$, $\phi = p_z d + \pi/6$. Projection of this spiral onto the momentum plane $q = 0$ determines the area of a flat band for surface states[9] in the limit $N \to \infty$. If only $\gamma_4 = 0$ while $\gamma_3 \neq 0$, equation $\epsilon = 0$ for $\mu = 0$ can still be shown to give a Fermi surface in the form of a (corrugated) spiral whose projection determines the surface flat band.[20] This is because the γ_3 interaction preserves the same topological invariant at the Fermi surface:[9] The full Hamiltonian obeys the same anticommutation rule $[\hat{\sigma}_z,(\hat{H}^{(0)} + \hat{H}^{(1)} + \hat{H}^{(3)})]_+ = 0$ as the initial Hamiltonian $\hat{H}^{(0)} + \hat{H}^{(1)}$. Since γ_3 does not destroy the flat band, we restrict our analytical consideration to the case when only γ_4 is nonzero while $\gamma_3 = 0$. However, our numerical analysis is carried out using the full Hamiltonian. The results are displayed in Fig. 1, along with the corresponding analytical approximations and DFT calculations.

Surface states have complex $p_z = p'_z + ip''_z$ and decay into the bulk. For $\gamma_3 = 0$ Eq. (2) in the particle channel,

$$v_F(\hat{\boldsymbol{\sigma}}\cdot\mathbf{p})\hat{u}_n(\mathbf{p}) - \gamma_1\left[e^{i\frac{\pi}{6}}\hat{\sigma}_-\hat{u}_{n+1} + e^{-i\frac{\pi}{6}}\hat{\sigma}_+\hat{u}_{n-1}\right]$$
$$+\tilde{\gamma}_4\left[e^{i\frac{\pi}{6}}v_F p_-\hat{u}_{n+1} + e^{-i\frac{\pi}{6}}v_F p_+\hat{u}_{n-1}\right] = (\epsilon+\mu)\hat{u}_n, \tag{3}$$

for low energies has a solution in the form

$$\hat{u}_n = Ce^{i(\phi-\frac{\pi}{6})(n-1-\frac{N}{2})} \times\left[\tilde{p}^{n-1}\begin{pmatrix}1\\ \zeta e^{i\phi}\end{pmatrix}A_+ + \tilde{p}^{N-n}\begin{pmatrix}\zeta\\ e^{i\phi}\end{pmatrix}A_-\right], \tag{4}$$

where $\tilde{p} = p/p_{\rm FB}$, $p_{\rm FB} = \gamma_1/v_F$, and

$$\zeta = \tilde{p}[(\epsilon+\mu)/\gamma_1 - \tilde{\gamma}_4(\tilde{p}^2+1)]/(\tilde{p}^2-1). \tag{5}$$

Here the out-of-plane momentum $p'_z d = \phi - \pi/6$ while $e^{\pm p''_z d} = \tilde{p}$. The overall normalization C is found from $d\sum_{n=1}^{N}[\mathrm{Tr}\,\hat{u}^\dagger_n\hat{u}_n] = 1$. For large N this gives $|C|^2 = d^{-1}[1-\tilde{p}^2]$ provided $|A^+|^2 + |A^-|^2 = 1$.

At the outermost layers, the components in Eq. (3) which do not have γ_1 couple the constants A^+ and A^- and determine the surface states. For $\xi_p,\epsilon \ll \gamma_1$,

$$\epsilon_p = \mu_p \pm \xi_p(1-\tilde{p}^2),\ \ \xi_p = \gamma_1\tilde{p}^N, \tag{6}$$

$$\mu_p = p^2/2m^* - \mu,\ \ m^* = \gamma_1/\left(4\tilde{\gamma}_4 v_F^2\right). \tag{7}$$

The interaction γ_4 breaks the symmetry between the conduction and valence bands in a way similar to a shift in μ due to doping. The spectrum ϵ_p has a quadratic dispersion with the effective mass m^* on a background of a much weaker high-order dispersion ξ_p. The latter transforms into a flat band $\xi_p = 0$ with a radius $p < p_{\rm FB}$ for an infinite number of layers, $N \to \infty$. The effective mass is much larger than the characteristic band mass m_3 in 3D graphite. Indeed, we have $m^*/m_3 \sim \gamma_1/\gamma_4$ where we estimate $\hbar^2/(m_3 a_0^2) \sim \gamma_0$ as the conduction band width in graphite. We see that $m^*/m_3 \gg 1$. This dispersion is compared with the results of numerical diagonalization of $H(\mathbf{K},\mathbf{p})$ in Fig. 1 using $\tilde{\gamma}_3 = 0.066$ and $\tilde{\gamma}_4 = 0.016$.

BdG equations are constructed using the particle and hole Hamiltonians of Eq. (1) coupled through the superconducting-order-parameter field Δ. As distinct from the quasiparticle energy measured from the chemical potential upwards, $E = \mu + \epsilon$, the energy of holes is measured from μ downwards, $E = \mu - \epsilon$. We have

$$\sum_m \check{\tau}_3 \otimes [\hat{H}_{nm}(\mathbf{K},\mathbf{p}) - \mu\delta_{nm}]\check{\Psi}_m + \check{\Delta}_n\check{\Psi}_n = \epsilon\check{\Psi}_n. \quad (8)$$

Here we introduce objects in the Nambu space

$$\check{\Delta}_n = \begin{pmatrix} 0 & \Delta_n \\ \Delta_n^* & 0 \end{pmatrix}, \ \check{\Psi}_n = \begin{pmatrix} \hat{u}_n \\ \hat{v}_n \end{pmatrix}, \ \check{\tau}_3 = \begin{pmatrix} 1 & 0 \\ 0 & -1 \end{pmatrix}.$$

Whereas more complicated symmetries are also possible, below we assume for simplicity s-wave superconducting pairing. Each component of the Nambu vector $\check{\Psi}_n$ is a pseudospinor. For analytical consideration we assume that $\Delta_n = 0$ for $n \neq 1, N$. This is justified by the numerical solution of the self-consistency equation using the full BdG equations.[14,20] In this case, Eq. (8) for $n \neq 1, N$ does not contain Δ, so that one can use the normal-state solution, Eq. (4), where we have Nambu vectors $\check{A}^{\pm} = (A^{\pm}, B^{\pm})^T$ instead of the corresponding scalars, and the Nambu matrix $\check{\zeta}$, Eq. (5), with $\check{\tau}_3\epsilon$ instead of ϵ.

At the outermost layers, the terms with $\hat{u}_0$, $\hat{v}_0$ and $\hat{u}_{N+1}$, $\hat{v}_{N+1}$ in Eq. (8) disappear. We find

$$\check{\tau}_3\xi_p\check{A}^- = (\tilde{\epsilon} - \check{\tau}_3\tilde{\mu}_p)\check{A}^+ - \check{\Delta}_1\check{A}^+, \quad (9)$$

$$\check{\tau}_3\xi_p\check{A}^+ = (\tilde{\epsilon} - \check{\tau}_3\tilde{\mu}_p)\check{A}^- - \check{\Delta}_N\check{A}^-, \quad (10)$$

where $\tilde{\epsilon} = \epsilon(1-\tilde{p}^2)^{-1}$, $\tilde{\mu}_p = \mu_p(1-\tilde{p}^2)^{-1}$. Equations (9) and (10) provide the surface-state spectrum and determine four independent surface states.

If $\Delta_1 = \Delta_N$, the spectrum is $\tilde{\epsilon}^2 = (\tilde{\mu}_p \pm \xi_p)^2 + |\Delta|^2$. If the number of layers N is large, $\xi_p \to 0$ for $p < p_{\rm FB}$, the two surface states decouple, yielding $\tilde{\epsilon}^2 = \tilde{\mu}_p^2 + |\Delta|^2$ at each surface. In this case, Eq. (9) at layer $n = 1$ yields $A^+ = U$, $B^+ = V$ or $A^+ = V$, $B^+ = U$, where

$$U = 2^{-\frac{1}{2}}[1 + \tilde{\mu}_p/\tilde{\epsilon}]^{\frac{1}{2}}, \ V = 2^{-\frac{1}{2}}[1 - \tilde{\mu}_p/\tilde{\epsilon}]^{\frac{1}{2}}. \quad (11)$$

Surface superconductivity. The gap at a layer n in the sample is determined by the mean-field self-consistency equation with a 3D coupling potential W. As was shown in Ref. 14, the surface states dominate over the bulk states due to a much larger DOS. Therefore, even though the potential W is nonzero and constant for all the layers, the self-consistent order parameter is concentrated only near the surfaces and decays rapidly into the bulk due to the structure of the basis wave functions. For a large number of layers when $\xi_p = 0$, the self-consistency equation for the gap value at the surface takes the form

$$1 = \frac{W}{d}\int_{\rm FB}\frac{d^2p}{(2\pi\hbar)^2}\frac{(1-\tilde{p}^2)}{\tilde{\epsilon}}\tanh\frac{\epsilon}{2T}. \quad (12)$$

Here we used Eq. (11) to find the integrand, and the integration is carried out over momenta within the flat band, $p < p_{\rm FB}$. This is the central result of this communication. We stress that it is based on the band structure of RHG along with the same assumptions as the standard BCS model. The superconducting coupling is described by the energy $g = (W/d)p_{FB}^2/\hbar^2$. It can also be expressed in terms of the usual BCS coupling constant $\lambda = \nu_3 W$ where $\nu_3 = m_3 p_{3F}/2\pi^3\hbar^3$ is the 3D density of states and p_{3F} is the Fermi momentum in 3D graphite. Assuming the conduction band width in 3D graphite of the order of γ_0 we have $g/\gamma_1 \sim \lambda(\gamma_1/\gamma_0)$ if $\hbar/a_0 p_{3F} \sim 1$.

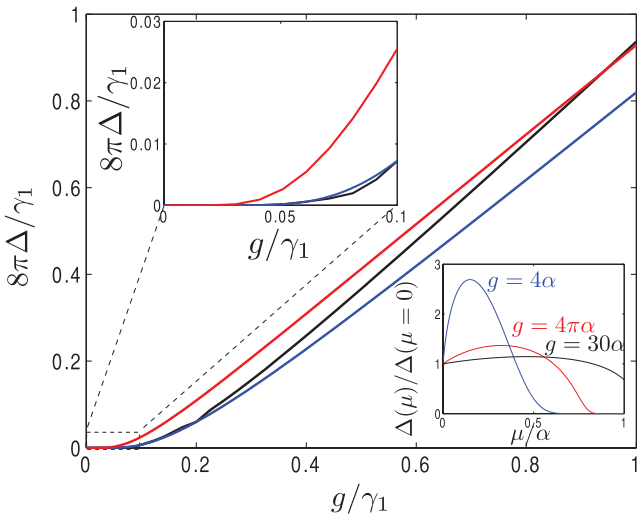

FIG. 2. (Color online) Self-consistent surface gap vs coupling g. The black line (in the middle) shows the results based on the exact diagonalization of the BdG equations for $N = 20$ with $\mu = 0$, the blue (bottom) line is Eq. (12) at $\mu = 0$, and the red (top) line corresponds to $\mu = \mu_{\rm opt}$ that maximizes Δ for given g. For large g, the gap tends towards the flat-band limit $\Delta \propto g$. For $g \lesssim 4\pi\alpha$ (upper inset), the gap is exponentially suppressed, $\Delta \propto \exp(-4\pi\alpha/g)$. The lower inset shows the (normalized) gap as a function of μ for a few values of g.

The overall behavior of Δ vs the coupling energy is plotted in Fig. 2. The quadratic dispersion comes with an energy scale $\alpha = 2\tilde{\gamma}_4\gamma_1$, which determines a crossover between exponentially suppressed and flat-band superconductivity. For $g \gg 4\pi\alpha$ and for zero doping, Eq. (12) yields the flat-band result,[14] $\Delta = g/8\pi$ for $T = 0$, and the critical temperature satisfying $\Delta = 3k_BT_C$. Due to its linear dependence on the interaction strength, *the critical temperature is proportional to the area of the flat band and can be essentially higher than that in the bulk*. For large values of the coupling constant g, Δ penetrates further into the bulk,[20] and the surface superconductivity is transformed into bulk superconductivity for $g \approx 8\pi\gamma_1$. Doping in the flat-band regime destroys the surface superconductivity.[14] Both Δ_0 and T_c vanish at the critical doping level $|\mu| = 2k_BT_c$.

For $g \ll 4\pi\alpha$ the weak dispersion Eq. (6) with a heavy mass m^* dominates. The integral in Eq. (12) is logarithmic which results in a BCS-like expression (for $T = 0$)

$$\Delta = [\alpha^2/(\alpha - \mu)]e^{-1/\lambda_2}, \quad \lambda_2 = g(1-\mu/\alpha)^2/4\pi\alpha,$$

where $\alpha = 2\gamma_1\tilde{\gamma}_4$. The estimate for g gives $\lambda_2 \sim \lambda(\gamma_1/\gamma_4)$. *This is a much larger coupling constant than λ for bulk superconductivity*. The gap disappears at $\mu = \alpha$. The crossover from the BCS-like to the flat-band regime occurs at $g \sim 4\pi\alpha$ and $\Delta \sim \alpha$. The coherence length $\xi_0 = \hbar v_g/\Delta \sim a_0(\gamma_0/\gamma_1)e^{1/\lambda_2}$ is much longer than the interatomic distance a_0. These analytical results are compared in Fig. 2 to the numerical solution of the

self-consistency equation using the full Hamiltonian, Eq. (8). We see that the gap in the intermediate region $\alpha \sim g$ is enhanced by an optimum doping; i.e., the critical temperature is very sensitive to the presence of impurities (lower inset in Fig. 2). This complies with the experimental results for doped graphite.[16]

Effect of fluctuations. The quality of the mean-field approximation is determined by the Ginzburg number Gi which is a measure of the relative magnitude of order-parameter fluctuations. For usual 3D superconductors Gi $\ll 1$ due to a small ratio of the critical temperature to characteristic energy of electrons (i.e., the Fermi energy). Here we demonstrate that the mean-field approach also works well when the quadratic dispersion dominates over the flat band. In this case the fluctuation free energy density for T not too close to T_c is $F_1 \sim \nu_2 \Delta_1^2/2$, where $\nu_2 = m^*/2\pi\hbar^2$ is the 2D DOS with the effective mass m^* from Eq. (7). The energy of an area $\pi\xi_0^2$ with a radius of $\xi_0 = \hbar v_g \Delta_0^{-1}$ is $\mathcal{F}_1 \sim \pi\xi_0^2 F_1 = \tilde{\gamma}_4\gamma_1(\Delta_1^2/\Delta_0^2)$, where Δ_0 is the mean-field gap. Since $\mathcal{F}_1 \sim T$ we find $\Delta_1^2/\Delta_0^2 = \mathrm{Gi} \sim T_c/\tilde{\gamma}_4\gamma_1$. When the quadratic dispersion dominates, one has $T_c \ll \gamma_1\tilde{\gamma}_4$ with $\mathrm{Gi} = e^{-1/\lambda_2} \ll 1$. Thus the average fluctuation of the order parameter is small compared to its mean-field value.[23] However, at the crossover to the flat-band regime, Gi ~ 1 and the mean-field approach is not exact. We use it only as an initial step towards a full theory of high-temperature surface superconductivity. We stress that the surface superconductivity here appears in a sample that is three-dimensional in other respects. Therefore, Coulomb repulsion is screened and can be neglected. Other graphene-specific phenomena such as sheet corrugations and fluctuating electron-hole puddles do not seem to be relevant either.

Summary. RHG is a promising candidate for high-temperature surface superconductivity due to its (approximate) topologically protected flat band. In general, flat bands are susceptible to instabilities with respect to some other ordered states; for example, a magnetic state could also be possible. Being interested here in superconductivity and supported by the experimental evidence,[16–19] we assume that superconductivity dominates and leave the problem of interplay between various instabilities to further work. Besides surfaces, superconductivity may arise around stacking faults and interfaces between different stackings of graphite, as long as the system contains more than a few layers of RHG embedded inside the Bernal phase.[20] Recent observations of high T_c in graphite[16–19] are compatible with surface or interface superconductivity described by our theory. Our predictions can be used for search or for an artificial fabrication of layered and/or twinned systems with high- and even room-temperature superconductivity. With the hopping parameters used above, the crossover between the flat-band and BCS-like regimes takes place around $g_c \sim 4\pi\alpha \approx 0.39\gamma_1 \approx 0.15$ eV (see Fig. 2 and Ref. 22) corresponding to the mean-field $T_c(g_c) \approx 20$ K. For $g > g_c$ we find $T_c \sim (g/\gamma_1) \times 50$ K. This is much greater than the bulk gap expected for the same magnitude of coupling.

Acknowledgments. We thank G. Volovik for helpful comments and the collaboration that initiated this project. We also acknowledge fruitful discussions with F. Mauri. This work is supported in part by the Academy of Finland through its Centre of Excellence Program (Projects No. 250280 and No. 251748) and by the European Research Council (Grant No. 240362-Heattronics).

[1] V. A. Khodel and V. R. Shaginyan, Pis'ma Zh. Eksp. Teor. Fiz. **51**, 488 (1990) [JETP Lett. **51**, 553 (1990)].

[2] G. E. Volovik, Pis'ma Zh. Eksp. Teor. Fiz. **53**, 208 (1991) [JETP Lett. **53**, 222 (1991)].

[3] V. R. Shaginyan, M. Ya. Amusia, A. Z. Msezane, and K. G. Popov, Phys. Rep. **492**, 31 (2010).

[4] Z. Gulacsi, A. Kampf, and D. Vollhardt, Phys. Rev. Lett. **105**, 266403 (2010).

[5] T. T. Heikkilä, N. B. Kopnin, and G. E. Volovik, Pis'ma Zh. Eksp. Teor. Fiz. **94**, 252 (2011) [JETP Lett. **94**, 233 (2011)].

[6] S. Ryu and Y. Hatsugai, Phys. Rev. Lett. **89**, 077002 (2002).

[7] A. P. Schnyder and Shinsei Ryu, Phys. Rev. B **84**, 060504(R) (2011); P. M. R. Brydon, A. P. Schnyder, and C. Timm, *ibid*. **84**, 020501(R) (2011).

[8] F. Guinea, A. H. Castro Neto, and N. M. R. Peres, Phys. Rev. B **73**, 245426 (2006).

[9] T. T. Heikkilä and G. E. Volovik, Pis'ma Zh. Eksp. Teor. Fiz. **93**, 63 (2011) [JETP Lett. **93**, 59 (2011)].

[10] Kin Fai Mak, Jie Shan, and T. F. Heinz, Phys. Rev. Lett. **104**, 176404 (2010).

[11] B. Dora, J. Kailasvuori, and R. Moessner, Phys. Rev. B **84**, 195422 (2011).

[12] N. B. Kopnin and M. M. Salomaa, Phys. Rev. B **44**, 9667 (1991).

[13] G. E. Volovik, Pis'ma Zh. Eksp. Teor. Fiz. **93**, 69 (2011) [JETP Lett. **93**, 66 (2011)].

[14] N. B. Kopnin, T. T. Heikkilä, and G. E. Volovik, Phys. Rev. B **83**, 220503 (2011).

[15] N. B. Kopnin, Pis'ma Zh. Eksp. Teor. Fiz. **94**, 81 (2011) [JETP Lett. **94**, 81 (2011)].

[16] R. R. da Silva, J. H. S. Torres, and Y. Kopelevich, Phys. Rev. Lett. **87**, 147001 (2001).

[17] P. Esquinazi, N. García, J. Barzola-Quiquia, P. Rödiger, K. Schindler, J.-L. Yao, and M. Ziese, Phys. Rev. B **78**, 134516 (2008); S. Dusari, J. Barzola-Quiquia, and P. Esquinazi, J. Supercond. Novel Magn. **24**, 401 (2011).

[18] A. Ballestar, J. Barzola-Quiquia, and P. Esquinazi, New J. Phys. **15**, 023024 (2013).

[19] T. Scheike, W. Böhlmann, P. Esquinazi, J. Barzola-Quiquia, A. Ballestar, and A. Setzer, Adv. Mater. **24**, 5826 (2012).

[20] N. B. Kopnin and T. T. Heikkilä, arXiv:1210.7075.

[21] A. H. Castro Neto, F. Guinea, N. M. R. Peres, K. S. Novoselov, and A. K. Geim, Rev. Mod. Phys. **81**, 109 (2009); D. P. Arovas and F. Guinea, Phys. Rev. B **78**, 245416 (2008); J. W. McClure, Carbon **7**, 425 (1969).

[22] See Supplemental Material at http://link.aps.org/supplemental/10.1103/PhysRevB.87.140503 for more information on our density functional calculations.

[23] On large distances, the system may also undergo a Berezinskii-Kosterlitz-Thouless transition to a disordered vortex state. Detailed analysis of this transition would require calculating the supercurrent through RHG, a task for a future work.